J Sol-Gel Sci Technol (2010) 53:535–541
DOI 10.1007/s10971-009-2128-6

ORIGINAL PAPER

Synthesis, characterization of B-doped TiO_2 nanotubes with high photocatalytic activity

Lixue Deng · Yinglei Chen · Meiyu Yao · Shurong Wang · Baolin Zhu · Weiping Huang · Shoumin Zhang

Received: 30 September 2009 / Accepted: 3 December 2009 / Published online: 18 December 2009

Abstract B-doped TiO_2 nanotubes (B/TiO_2 NTs) were prepared by the combination of sol–gel process with hydrothermal treatment. The prepared catalysts were characterized by XRD, TEM and XPS. The photocatalytic activity of B/TiO_2 NTs was evaluated through the photodegradation of aqueous methyl orange. The results demonstrated that the 1.5% B/TiO_2 NTs calcined at 300 °C possessed the best photocatalytic activity. Compared with pure TiO_2 nanotubes, the doping with B significantly enhanced the photocatalytic efficiency.

Keywords B-doped TiO_2 · Nanotubes · Photocatalytic activity

1 Introduction

Semiconductor photocatalysis is a promising technology in air purification, water disinfection, hazardous waste remediation, and water purification [1]. Among various candidates, TiO_2 is proved to be the most suitable catalyst in view of its strong oxidation activity. However, its photocatalytic oxidation rates for many target pollutants are too slow to be of practical utility [2–4]. Doping with suitable nonmetals has been attempted to improve its performances. Many nonmetals, such as nitrogen [5], carbon [6, 7], sulfur [8], phosphorus [9], fluorine [10] and boron [11], etc. have been used to modify the properties of TiO_2.

L. Deng · Y. Chen · M. Yao · S. Wang · B. Zhu · W. Huang · S. Zhang (✉)
Department of Chemistry, Nankai University, 300071 Tianjin, China
e-mail: zhangsm@nankai.edu.cn

Among them, boron doping is observed to be a potential method and improved performance can be obtained. For example, In et al. [12] reported that an optimal level of boron doping induces a larger absorption of visible light and enhanced photocatalytic activity. Su et al. [13] revealed that B-doped TiO_2 nanotubes that were prepared by chemical vapor deposition (CVD) displayed stronger absorption in both UV and visible range. The experimental results of Chen et al. [14] indicated that all B-doped TiO_2 nanoparticles prepared by sol–gel method showed higher photocatalytic activity than pure TiO_2 sample in the photocatalytic reaction of nicotinamide adenine dinucleotide (NADH) regeneration under UV light irradiation. Yang et al. also reported that B-doped anatase models were investigated by spin-polarized density functional theory. It is reported that the radii of the boron atom is very small and can site at an interstitical position. In this B-doped TiO_2 system, that B replacing an O atom induces some gap states close to the bottom of the conduction band, and may account for redshift of the absorption edge [11]. From these researches, it can be inferred that the photocatalytic activity of TiO_2 can be improved by the doping of boron.

Recently, extensive researches have been conducted on the synthesis and characterization of TiO_2 nanotubes because of their novel properties, such as unique shape, size confinement in radial-direction and large specific surface area [15–20]. Furthermore, the high sedimentation rate of the nanotubes facilitates their reuse as photocatalysts [21]. By modifying with different ions, the photocatalytic activity of the tubular TiO_2 can be improved. In our group, different elements, such as gold [22], platinum [23], palladium [24], nitrogen [25], Chromium [26], fluorine [10], have been used to modify the TiO_2 nanotubes and enhanced photocatalytic activity is obtained. However, to our knowledge, photocatalysis upon anatase B/TiO_2 NTs

has not been reported. Higher photocatalytic activity can be expected on the B/TiO_2 NTs. In this paper, B/TiO_2 NTs were prepared by using B-doped anatase TiO_2 powder as precursors. The products were characterized by XRD, TEM and XPS. Their photocatalytic activity under UV–Vis light irradiation was evaluated by the degradation of methyl orange.

2 Experimental

Tetrabutyl titanate ($C_{16}H_{36}O_4Ti$, AR), which was used as titanate (TiO_2) precursor, was purchased from Tianjin Kermel chemical Co., Ltd, China. Boric acid (H_3BO_3, AR), which was used as the doped agent, was purchased from Tianjin Guangfu chemical Co., Ltd, China. Ethanol (C_2H_5OH, AR), which was used as a solvent, was purchased from Tianjin Guangfu chemical Co., Ltd, China. All the reagents were used without any further purification.

2.1 Preparation of B/TiO_2 NTs

B-doped TiO_2 powder was prepared by the sol–gel route using tetrabutyl titanate and boric acid as the precursors. Under constant stirring, ethanol solution of tetrabutyl titanate was added drop-wise to the mixture of ethanol and a desired amount boric acid solution. The transparent sol was obtained when the mixture was hydrolyzed at room temperature for 2 h under vigorous stirring. Then, gel was obtained by aging the sol for 12 h at room temperature. The resulting gel was dried at 80 °C in oven for 12 h to remove the solvents and then calcined at 500 °C in muffle furnace for 3 h. Then the B-doped TiO_2 powder was obtained. The calculated boron concentrations were 1.0, 1.25, 1.5, 1.75%, respectively. Pure TiO_2 powder was synthesized with the same process except that distilled water instead of boric acid solution is used. Pure titanate nanotubes and doped nanotubes with different boron concentration were synthesized via a simple hydrothermal chemical process. 1.0 g B-doped TiO_2 powder or pure TiO_2 powder was mixed with 50 mL 10 mol/L NaOH aqueous solution in a Teflon vessel and maintained at 150 °C for 12 h. The resulting materials were washed with 0.1 mol/L HNO_3 solution and distilled water, respectively, and then dried at 80 °C overnight in an oven. After the prepared material was calcined at 300 °C for 2 h, B/TiO_2 NTs were obtained. The corresponding B concentrations obtained in the photocatalysts were expressed as wt%.

2.2 Samples characterization

The powder X-ray diffraction (XRD) experiments were carried out at room temperature using a Rigaku D/Max-2500 X-ray diffractometer (CuKα $\lambda = 0.154$ nm) to identify the crystal phase of the products. TEM images were obtained with a Philips T20ST transmission electron microscopy working at 200 kV. The charge state of doped TiO_2 at the surface was investigated by X-ray photoelectron spectroscopy (XPS) using an Al X-ray source (Al $K\alpha$-150W, Kratos Axis Ultra DLD).

2.3 Photoactivity measurement

The photocatalytic activity under UV–Vis light irradiation of the prepared catalysts was evaluated by the degradation rates of methyl orange (20 mg/L) in an aqueous solution (100 mL) containing 50 mg of sample. The reaction mixture was ultrasonically dispersed for 30 min, and then irradiated by using a 300 W High-Pressure Mercury Lamp under stirring. The radiation range of the High-Pressure Mercury Lamp is from 200 to 1,000 nm, and the full spectrum was used for experiments. After every given irradiation time, a sample of 5 mL suspension was withdrawn, centrifugated and filtered. The obtained solution was then measured for checking the residual concentration of methyl orange with a UV–Vis spectrophotometer (TU-1901) at 463.8 nm, which is the maximum absorption of methyl orange. The results are corrected for the decomposition of methyl orange in the absence of catalysts and for absorption of methyl orange on the catalyst. In the irradiation experiments, air or O_2 bubbling was not used.

3 Results and discussion

Figure 1 shows the XRD patterns of 1.5% B/TiO_2 NTs and pure TiO_2 nanotubes calcined at 300 °C for 2 h. Diffractions that are attributable to anatase TiO_2 are clearly detectable in pure TiO_2 nanotubes and B/TiO_2 NTs (JCPDS 21-1272). The diffraction peaks for boron or boron containing phases were not observed, which indicated that boron was highly dispersed on TiO_2, or XRD was not sensitive enough to detect such minor changes to TiO_2.

Figure 2 shows TEM images of 1.5% B/TiO_2 NTs. Tubular structures are clearly observed. Figure 2a indicates that nanotubes are hollow and open-ended. Their diameters are nearly uniform and their length is more than hundreds of nanometers, similar to the results reported by Kasuga et al. [15, 16]. Figure 2b shows the TEM image of the obtained B/TiO_2 NTs calcined at 300 °C for 2 h. It can be seen that most of the nanotubes keep their tubular shape after the calcination process.

Figure 3 shows the XPS survey spectra before and after Ar^+ etching of B/TiO_2 NTs with 1.5 wt% boron calcined at 300 °C for 2 h. There are Ti, O, B, and C on the surface of

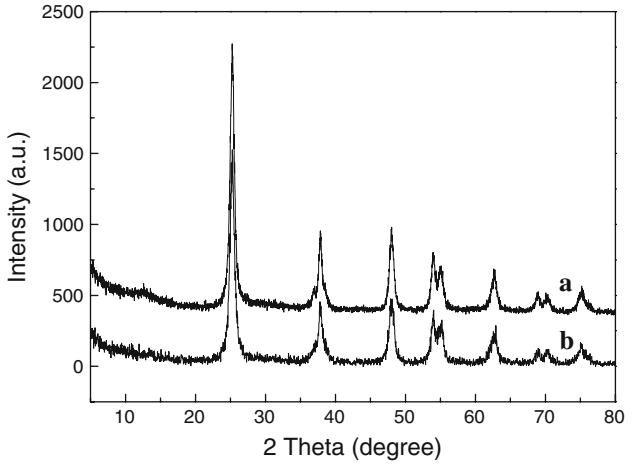

Fig. 1 XRD patterns of pure TiO_2 nanotubes (**a**) and 1.5% B/TiO_2 NTs (**b**) calcined at 300 °C

B/TiO_2 NTs. The presence of C element should mainly come from residual carbon from the organic precursors used in the sol–gel method and the adventitious hydrocarbon from XPS. It should be noted that the intensity of peak corresponding C 1s appeared in the sample after etching was obviously weaker than that appeared in the sample before etching, indicating that the adventitious hydrocarbon from XPS itself was partly removed by Ar^+ etching. The doping concentration of B analyzed by XPS was 1.15 wt% before etching and 0.61 wt% after etching, which implies that B dopant has a much higher concentration at the exterior than that at the interior of TiO_2 nanotubes. After the hydrothermal process, the B-doped nanoparticles turned into tubular structures and the doped boron was mainly dispersed in the outer layer of the nanotubes, which results in the difference of the boron concentration before and after Ar^+ etching. However, the measured concentrations are smaller than the calculated one. It should be attributed to the boron loss during the hydrothermal process.

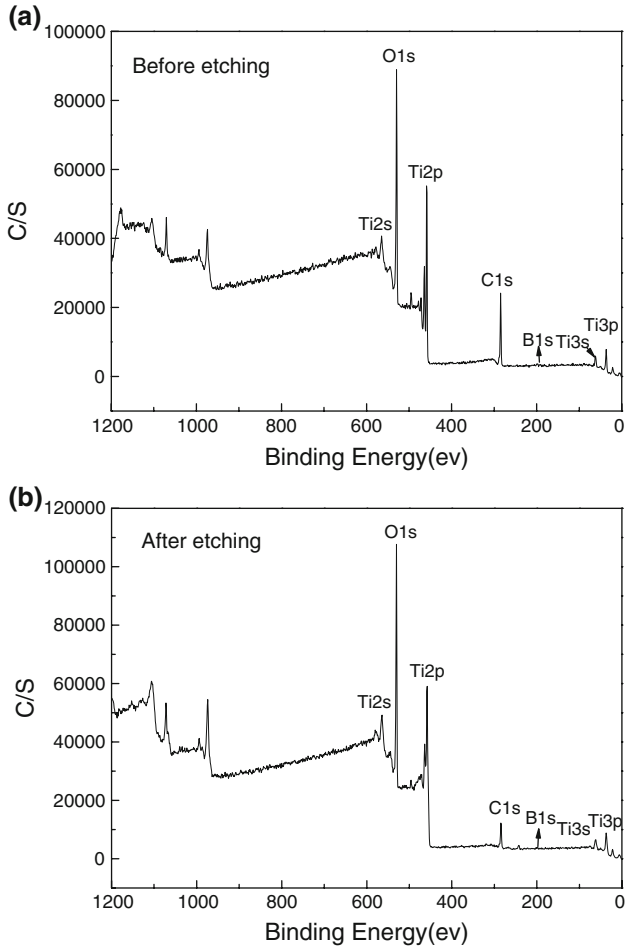

Fig. 3 XPS survey spectra of B/TiO_2 NTs before and after Ar^+ etching

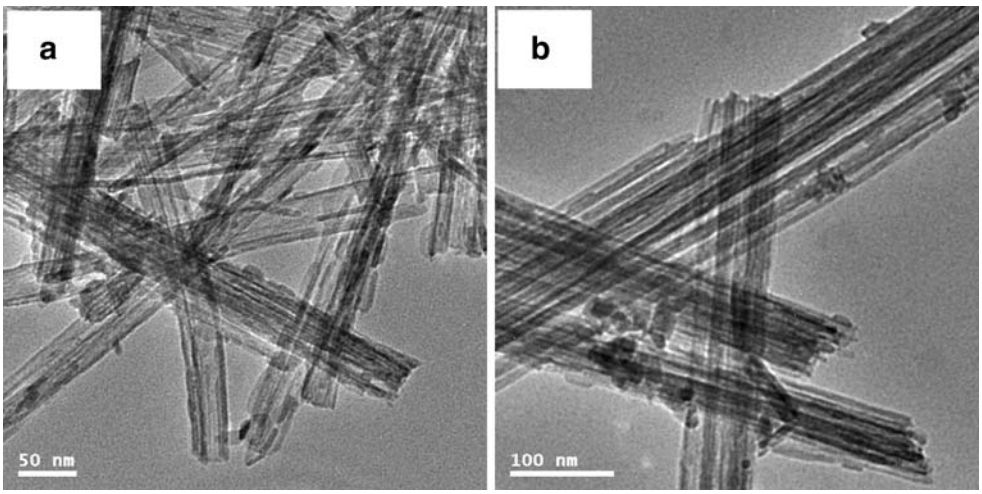

Fig. 2 TEM images of 1.5% B/TiO_2 NTs without calcination (**a**) and calcined at 300 °C (**b**)

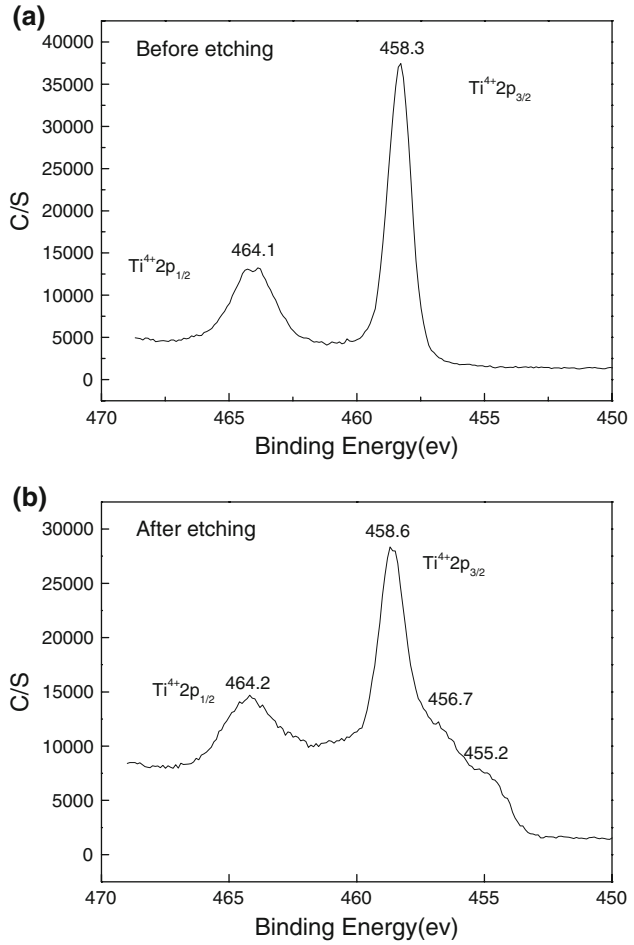

Fig. 4 High resolution XPS spectra of the Ti 2p region for the B/TiO_2 NTs before and after Ar^+ etching

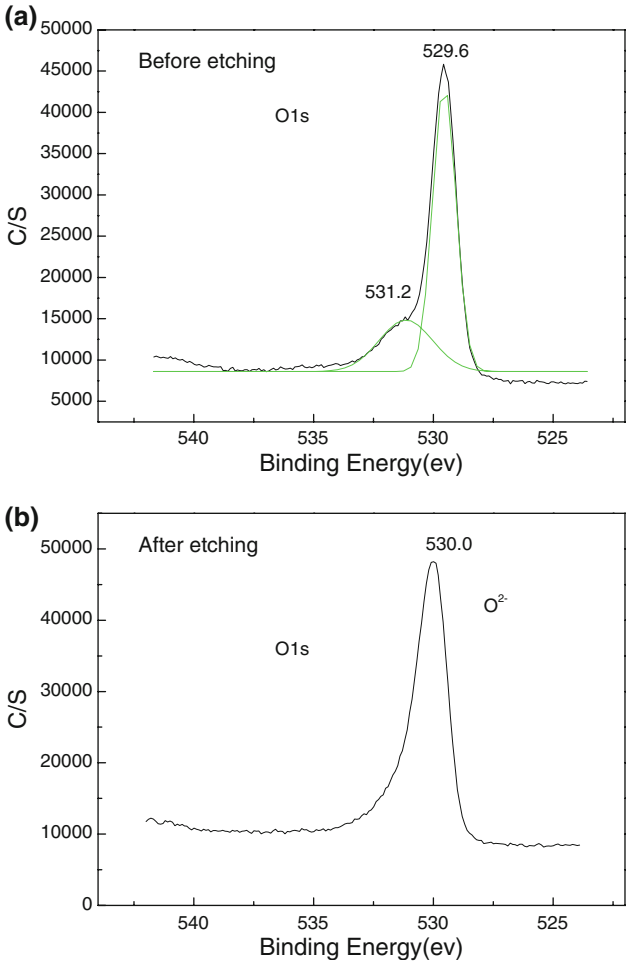

Fig. 5 High resolution XPS spectra of the O 1s region for the B/TiO_2 NTs before and after Ar^+ etching

Figure 4 shows the high resolution XPS spectra of Ti 2p. The Ti $2p_{1/2}$ and Ti $2p_{3/2}$ spin-orbital splitting photoelectrons are located at binding energies of 464.1 and 458.3 eV, respectively, which was in agreement with the values in the reported literatures [27, 28], showing the presence of Ti^{4+}. However, the surface spectrum of the etched sample revealed two shoulder regions. The peak at 456.7 and 455.2 eV should be ascribed to Ti^{3+} 2p3/2 and Ti^{2+} 2p3/2 in the sample, respectively [27]. The presence of low valence Ti might be attributed to Ar^+ etching.

Figure 5 shows the O 1s XPS spectra of B/TiO_2 NTs. The O 1s spectrum was asymmetric. The main peak of O 1s located at about 529.6 eV, corresponding to lattice oxygen of TiO_2. The shoulder located at 531.2 eV indicates a great amount of surface hydroxyl groups and chemical adsorbed oxygen [27, 28]. After Ar^+ etching treatment, the shoulder peak approximately disappeared. That indicates the removal of water and adsorbed oxygen from the TiO_2 surface.

Figure 6 shows the B 1s XPS spectra of B/TiO_2 NTs before Ar^+ etching. The B 1s region contains one peak at 191.6 eV. The standard binding energy of B 1s is 193.0 eV (B–O bond) in B_2O_3 or H_3BO_3 and 187.5 eV (B–Ti bond) in TiB_2. So the binding energy of B 1s is between that of B_2O_3 and TiB_2. This indicates the boron atom was probably incorporated into TiO_2 and the chemical environmental surrounding might be Ti–B–O [14, 29].

B-doping obviously affects light absorption characteristics of TiO_2, as shown in Fig. 7. The absorption spectra of the 1.5% B/TiO_2 NTs calcined at 300 °C for 2 h showed a stronger absorption in the UV–Visible range. Meanwhile, the absorption edge is changed from 407 nm (pure TiO_2 nanotubes) to 422 nm for B/TiO_2 NTs. It suggested that the incorporation of boron with TiO_2 induces an obvious red shift and makes the band gap energy smaller [30]. Yang et al. [11] reported that substitution B replacing an O atom induces some gap states close to the bottom of the conduction band and this may account for the redshift of the adsorption edge in TiO_2. The narrower band gap will facilitate the

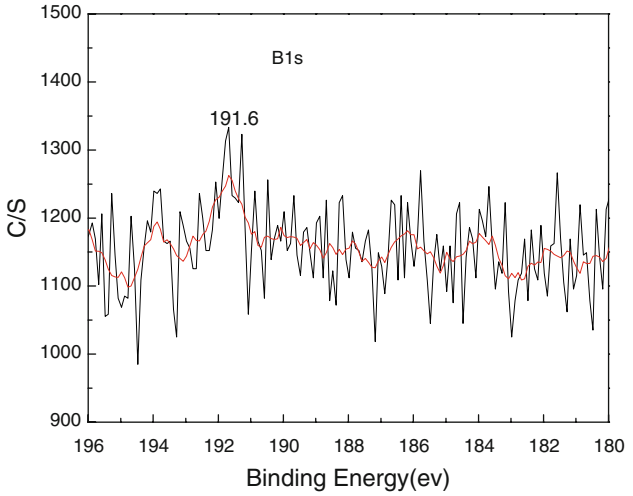

Fig. 6 High resolution XPS spectra of the B 1s region for the B/TiO_2 NTs before Ar^+ etching

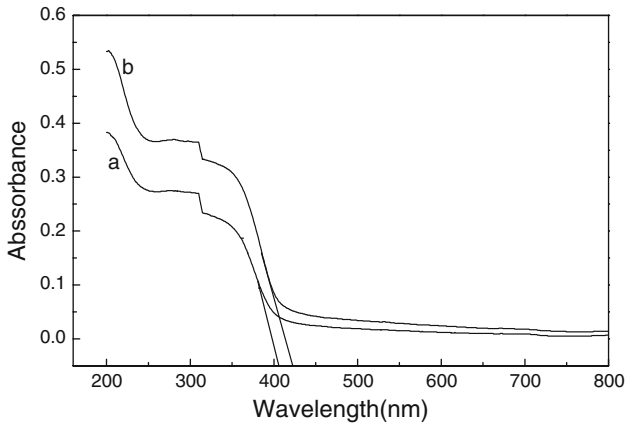

Fig. 7 UV–Vis absorption spectra of pure TiO_2 nanotubes (*a*) and B/TiO_2 NTs (*b*)

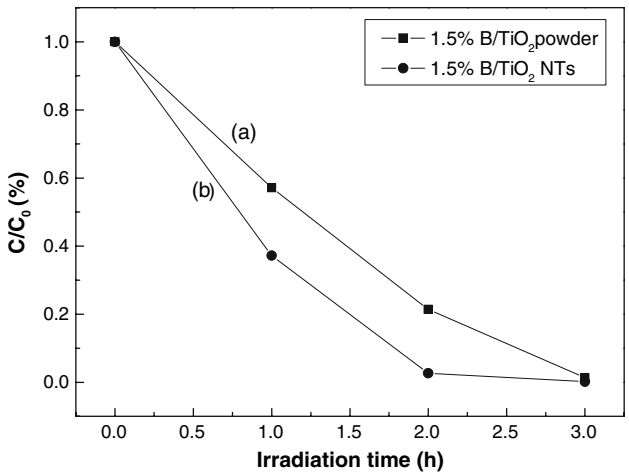

Fig. 8 Photocatalytic activity of 1.5% B/TiO_2 powder (**a**) and 1.5% B/TiO_2 NTs (**b**)

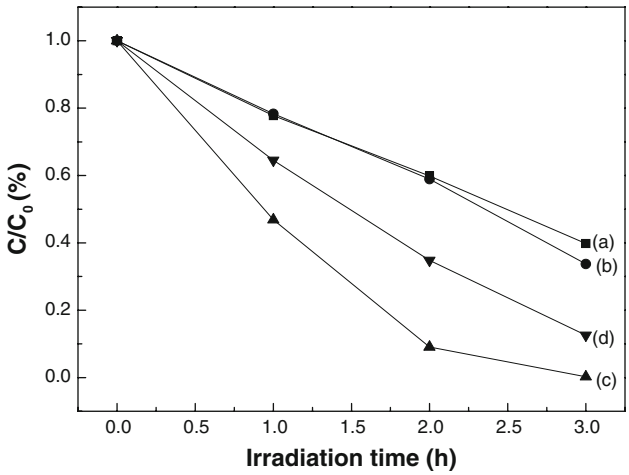

Fig. 9 Photodegradation of methyl orange by 1.25% B/TiO_2 NTs without calcination (*a*) and calcined at 200 °C (*b*), 300 °C (*c*), and 400 °C (*d*)

excitation of an electron from the valence band to the conduction band in the doped TiO_2 catalyst, and enhance the photocatalytic performance of TiO_2 consequently.

Figure 8 shows the degradation rates of methyl orange for 1.5% B/TiO_2 powder and 1.5% B/TiO_2 NTs calcined at 300 °C for 2 h. 78.2% of the methyl orange is degraded after 2 h irradiation in the presence of B/TiO_2 powder, while 97% of the methyl orange is degraded in the presence of B/TiO_2 NTs. Obviously, the photocatalytic activity of the B/TiO_2 NTs is better than that of B/TiO_2 powder. The reason is that TiO_2 nanotubes have their novel properties, such as unique shape, size confinement in radial-direction and large specific surface area [15–20]. These induce the better photocatalytic activity of the B/TiO_2 NTs than that of B/TiO_2 powder.

Calcination is an effective treatment method to enhance the photocatalytic activity of nanosized TiO_2 photocatalysts. Figure 9 shows the photocatalytic performance of B/TiO_2 NTs without calcination and calcined at different temperatures. As shown in Fig. 9, 60.3, 66.3, 99.7 and 87.4% of the methyl orange is degraded after 3 h irradiation in the presence of 1.25% B/TiO_2 NTs without calcination, calcined at 200, 300 and 400 °C, respectively. It is obviously that B/TiO_2 NTs without calcination show much lower photocatalytic activity. It can be attributed to the existence of titanate. When calcined at 200 °C, B/TiO_2 NTs show higher photocatalytic activity, which should due to the formation of anatase. After the calcination treatment, titanate in the nanotubes turn into anatase TiO_2 and higher photocatalytic activity is obtained. The B/TiO_2 NTs calcined at 300 °C possess the best photocatalytic activity. This result is also in accordance with the result reported by Zhang et al. [20]. The photocatalytic activity of B/TiO_2 NTs decreases with a

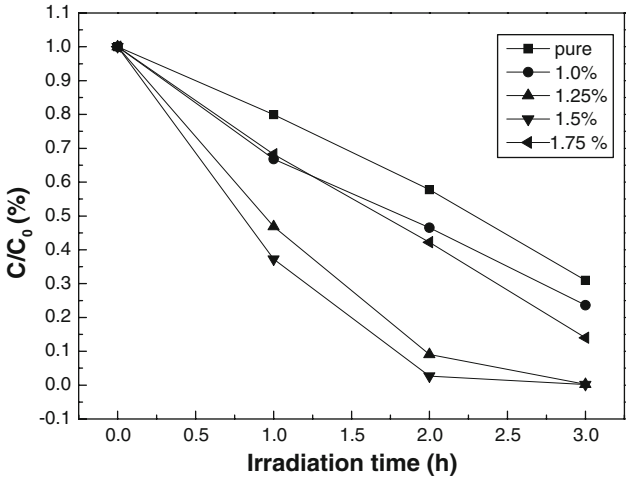

Fig. 10 The photocatalytic activity of B/TiO_2 NTs with various boron doping concentrations

further increase in calcination temperature (Fig. 9d). That is probably due to the agglomeration and sintering damage of nanotubes caused by calcination at high temperature [31].

Figure 10 shows the photodegradation of methyl orange for B/TiO_2 NTs as a function of B-doping concentration. All the catalysts were calcined at 300 °C. 69.1, 76.5, 99.7, 99.9, 86.1% of the methyl orange is degraded after 3 h irradiation in the presence of TiO_2 NTs with 0, 1.0, 1.25, 1.5, and 1.75% boron doping, respectively. It can be observed that B/TiO_2 NTs exhibit much higher photocatalytic activity for the photodegradation of methyl orange than pure TiO_2 nanotubes. The results reveal that the photocatalytic performance of TiO_2 NTs can be improved by the boron doping.

As has been reported, the doped-B atoms can promote the formation of oxygen vacancies [12]. The role of oxygen vacancies is to directly provide the sites of the formation of active species for photocatalytic reaction. The formation of $O_2^{\cdot -}$ upon chemisorbed oxygen or $OH^{\cdot}$ upon adsorbed water requires the presence of surface oxygen vacancies. The presence of Ti^{3+} also can apparently enhance the photocatalytic activity. The boron doping converts some Ti^{4+} to Ti^{3+} by charge compensation. The existence of a certain amount of Ti^{3+} can act as an active site to assist the adsorption of reactant and trap the photogenerated electron to reduce the recombination of photoexcited electrons and holes [14]. As a result, the photocatalytic activity of TiO_2 nanotubes is improved by boron doping.

4 Conclusions

B/TiO_2 NTs are prepared by the combination of sol–gel process with hydrothermal treatment. The prepared nanotubes are hollow and open-ended, and their length is more than hundreds of nanometers. Most of the nanotubes keep their tubular texture after the calcination process. B/TiO_2 NTs with 1.5% boron doping in the initial solution calcined at 300 °C possess the best photocatalytic activity. The high photocatalytic activity of B/TiO_2 NTs is ascribed to several beneficial effects produced by B-doping: intense absorption in the UV–Visible range and a red shift in the band gap transition, creation of oxygen vacancies, presence of Ti^{3+}, and so on.

Acknowledgments This work was supported by the National Natural Science Foundation of China (Grant No. 20771061), 973 Program (2005CB623607) and Research Fund for the Doctoral Program of Higher Education (200800551036).

References

1. Hoffmann MR, Martin ST, Choi W, Bahnemannt DW (1995) Chem Rev 95:69–96
2. Linsebigler AL, Lu GQ, Yates JT (1995) Chem Rev 95:735–758
3. Fujishima A, Rao TN, Tryk DA (2000) J Photochem Photobiol C Photochem Rev 1:1–21
4. Diebold U (2003) Surf Sci Rep 48:53–229
5. Asahi R, Morikawa T, Ohwaki T, Aoki K, Taga Y (2001) Science 293:269–271
6. Nakano Y, Morikawa T, Ohwaki T, Taga Y (2005) Appl Phys Lett 87:052111-1–052111-3
7. Choi Y, Umebayashi T, Yoshikawa M (2004) J Mater Sci 39:1837–1839
8. Tian FH, Liu CB (2006) J Phys Chem B 110:17866–17871
9. Yu HF (2007) J Phys Chem Solids 68:600–607
10. Yu Y, Wu HH, Zhu BL, Wang SR, Huang WP, Wu SH, Zhang SM (2008) Catal Lett 121:165–171
11. Yang KS, Dai Y, Huang BB (2007) Phys Lett B 76:195201–195206
12. In S, Orlov A, Berg R, García F, Jimenez SP, Tikhov MS, Wright DS, Lambert RM (2007) J Am Chem Soc 129:13790–13791
13. Su YL, Han S, Zhang XW, Chen XQ, Lei LC (2008) Mater Chem Phys 110:239–246
14. Chen DM, Yang D, Wang Q, Jiang ZY (2006) Ind Eng Chem Res 45:4110–4116
15. Kasuga T, Hiramatsu M, Hoson A, Sekino T, Niihara K (1998) Langmuir 14:3160–3163
16. Kasuga T, Hiramatsu M, Hoson A, Sekino T, Niihara K (1999) Adv Mater 11:1307–1311
17. Yao BD, Chan YF, Zhang XY, Zhang WF, Yang ZY, Wang N (2003) Appl Phys Lett 82:281–283
18. Yang JJ, Jin ZS, Wang XD, Li W, Zhang JW, Zhang SL, Guo XY, Zhang ZJ (2003) Dalton Trans 20:3898–3901
19. Bavykin DV, Parmon VN, Lapkin AA, Walsh FC (2004) J Mater Chem 14:3370–3377
20. Zhang M, Jin ZS, Zhang JW, Guo XY, Yang JJ, Li W, Wang XD, Zhang ZJ (2004) J Mol Catal A Chem 217:203–210
21. Li H, Zhu BL, Feng YF, Wang SR, Zhang SM, Huang WP (2007) J Solid State Chem 180:2136–2142
22. Zhu BL, Li KR, Feng YF, Zhang SM, Wu SH, Huang WP (2007) Catal Lett 118:55–58
23. Zhu BL, Li KR, Wang SR, Zhang SM, Wu SH, Huang WP (2008) J Dispers Sci Technol 29:1408–1411
24. Zhu BL, Li KR, Zhou J, Wang SR, Zhang SM, Wu SH, Huang WP (2008) Catal Commun 9:2323–2326

25. Chen YY, Zhang SM, Yu Y, Wu HH, Wang SR, Zhu BL, Huang WP, Wu SH (2008) J Dispers Sci Technol 29:245–249
26. Zhang SM, Chen YY, Yu Y, Wu HH, Wang SR, Zhu BL, Huang WP, Wu SH (2008) J Nanopart Res 10:871–875
27. Liu HM, Yang WS, Ma Y, Cao YA, Yao JN, Zhang J, Hu TD (2003) Langmuir 19:3001–3005
28. Nagaveni K, Hegde MS, Ravishankar N, Subbanna GN, Madras G (2004) Langmuir 20:2900–2907
29. Zhao W, Ma WH, Chen CC, Zhao JC, Shuai ZG (2004) J Am Chem Soc 126:4782–4783
30. Lu N, Quan X, Li JY, Chen S, Yu HT, Chen GH (2007) J Phys Chem C 111:11836–11842
31. Xu JC, Lu M, Guo XY, Li HL (2005) J Mol Catal A Chem 226:123–127